

# Vanilla Group Equivariant Vision Transformer: Simple and Effective

Jiahong Fu<sup>1</sup> Qi Xie<sup>1</sup> Deyu Meng<sup>1</sup> Zongben Xu<sup>1</sup>

<sup>1</sup> School of Mathematics and Statistics, Xi'an Jiaotong University, Xi'an, China

## Abstract

*Incorporating symmetry priors as inductive biases to design equivariant Vision Transformers (ViTs) has emerged as a promising avenue for enhancing their performance. However, existing equivariant ViTs often struggle to balance performance with equivariance, primarily due to the challenge of achieving holistic equivariant modifications across the diverse modules in ViTs—particularly in harmonizing the Self-Attention mechanism with Patch Embedding. To address this, we propose a straightforward framework that systematically renders key ViT components, including patch embedding, self-attention, and positional encodings, and Down/Up-Sampling, equivariant, thereby constructing ViTs with guaranteed equivariance. The resulting architecture serves as a plug-and-play replacement that is both theoretically grounded and practically versatile, scaling seamlessly even to Swin Transformers. Extensive experiments demonstrate that our equivariant ViTs consistently improve performance and data efficiency across a wide spectrum of vision tasks.*

## 1. Introduction

Vision Transformers (ViTs) [15, 26, 41] have become a dominant architecture in computer vision, achieving state-of-the-art performance across diverse tasks including image classification, detection, segmentation, and restoration. This success stems primarily from the self-attention mechanism, which excels at capturing long-range dependencies and has established ViTs as a foundational paradigm surpassing convolutional and fully-connected networks in modeling global context.

Current research [9, 11, 13, 14, 35] have shown that proper inductive biases are important for enhancing the performance of deep network architectures, including the Self-Attention mechanism. Particularly, in computer vision tasks, transformations like image translation, rotation, and mirroring usually do not affect the final image recognition and classification results [1, 8], which naturally attribute to the most common used inductive bias: symmetry priors present in both the local features and global semantics un-

der the aforementioned transformations. However, standard Vision Transformers (ViTs) have not explicitly embedded such inductive biases into their design. Consequently, current ViT models typically rely on massive datasets and extensive data augmentation to implicitly learn these symmetries—a process that demands substantial data and computational resources while still failing to guarantee the systematic embedding of symmetry priors [14, 16, 35].

It is noteworthy that in recent years, the emergence of equivariant CNN architectures [8, 38, 53] has achieved remarkable success in embedding symmetry priors, demonstrating that directly designing equivariant model architectures offers unique advantages in parameter efficiency and performance enhancement, compared to learning symmetries from training data. This insight inspires the recognition that designing guaranteed equivariant architecture for ViTs is a highly promising research direction.

However, replicating the successful design of equivariant architectures from CNNs to Vision Transformers (ViT) has been proven to be challenging. Most existing approaches leverage the intrinsic permutation equivariance of self-attention [36, 55], yet this property is disrupted during patch embedding, forcing methods to operate directly on pixel-level features. This approach significantly compromises local feature representation and generally underperforms modern ViT architectures [15, 26, 41]. Furthermore, quadratic memory growth with image size limits processing to low-resolution inputs. Recent theoretical frameworks for ViT equivariance have been proposed [18, 21], but resulting implementations are often overly complex and fail to surpass standard ViT performance. More importantly, these methods differ too significantly from the original ViT, making them difficult to adapt to ViT variants, such as Swin-Transformers [26], which largely restricts their applicability.

The aforementioned methods' struggle in balancing performance and equivariance highlights two fundamental difficulties in designing equivariant ViTs: **(I) Effective equivariant designs that harmonize the Self-Attention mechanism with Patch Embedding remain elusive.** Unlike the convolution in CNNs, which is inherently equivariant to local translations, Self-Attention possesses long-range con-

nectivity and a more complex computational structure. This complexity makes its equivariant modification significantly more challenging, especially when patches themselves undergo rotations or reflections. **(II) A holistic equivariant framework for diverse other modules in ViTs is lacking.** Beyond the above two core components, standard Vision Transformers incorporate various other modules, such as positional encodings, Down/Up-Sampling layers(in Swin-Transformer), LayerNorm, all of which are essential for performance. All of these components must be made equivariant holistically to guarantee the equivariance of the entire architecture.

To address the aforementioned challenges, we explore a vanilla path to construct comprehensive equivariant framework for all common components in Vision Transformers, thereby constructing ViT architectures that are rigorously equivariant to  $\pi/2$  rotations and reflections. Our principal contributions are as follows:

(1) We propose a straightforward method to convert a standard Vision Transformer (ViT) into its rotation and reflection equivariant version. First, we employ an equivariant CNN-based patch embedding to lift the input domain, producing feature maps with an added group dimension. We then use equivariant linear layers [34, 54] to harmonize Self-Attention with the patch embedding in an equivariant manner. Furthermore, via judicious group-wise parameter sharing and a tailored feature reordering strategy, we redesign positional encodings and Resampling layers, forming a holistic equivariant framework for diverse ViT modules. As a result, our equivariant ViT acts as a plug-and-play replacement across applications, enabling potential performance gains and parameter reduction.

(2) For the first time, our method can be seamlessly and effectively applied to Swin Transformer, enhancing its performance. This successful adaptation significantly broadens the applicability and practicality of equivariant architectures, demonstrating our framework’s generality.

(3) Through rigorous theoretical analysis, we prove that the proposed framework maintains strict equivariance for both the overall network architecture and individual modules. Simultaneously, our theoretical findings indicate that the modified ViT architecture will possess an enhanced generalization capability.

(4) Extensive experiments across multiple benchmarks validate our method’s effectiveness in consistently improving performance and data efficiency across various tasks, from high-level recognition to low-level restoration. These results establish that explicit geometric symmetry embedding is crucial for developing more powerful and robust Vision Transformers.

## 2. Related Work

### 2.1. Vision Transformers

The Transformer architecture originally developed for NLP [42] has become foundational in computer vision. The Vision Transformer (ViT) [15] first adapted it by treating images as sequences of  $16 \times 16$  patches, revealing self-attention’s potential in vision tasks. However, ViT suffers from quadratic complexity and limited inductive bias, restricting its scalability and efficiency. The Swin Transformer [26, 27] addressed this with a hierarchical shifted-window design, enabling linear complexity while retaining global context, later extended to restoration tasks in SwinIR [25]. Beyond pure attention models, hybrids like CvT [49] integrate convolutional projections to embed spatial locality efficiently. Other approaches [16, 24, 45] use pyramidal structures for multi-scale modeling. Recently, Vision Transformers are increasingly tailored to specific tasks: SwinIR leverages hierarchy for restoration, while DETR [6] and SegFormer [52] adapt architectures for detection and segmentation.

### 2.2. Group Equivariant Neural Networks

Early attempts for exploring transformation symmetry priors in images primarily rely on data augmentation [20, 22, 40] and self-supervised learning frameworks [1, 13]. Recently, most works have primarily focused on embedding transformation equivariance directly into network architectures via equivariant module designs. Prior work in this direction is G-CNN [8], it achieves 90-degree rotation and mirror reflection equivariance. Since then various types of rotationally equivariant convolution [38, 48] networks have emerged. In recent years, research on the equivariance of Transformer model embeddings has been quite active. In recent years, there have been many efforts [5, 18, 21, 36, 55] to design equivariant vision transformers. Specifically, [36, 55] construct equivariant Self-Attention by a lifting positional encoding. [18] constructs an efficient equivariant attention layer and [21] design a sterrable ViT. Further, shift equivariant Transformer [14, 35] are beginning to attract attention.

## 3. Method

In this section, we first present the foundational concepts for equivariance and vision transformer architecture, and then provide the proposed equivariant ViT, as well as the theoretical analysis for equivariance error and generalization error.

### 3.1. Preliminaries

**Equivariance.** Equivariance of a mapping means that a transformation on the input will result in a predictable transformation on the output [10, 38, 53]. In this work, we focus on achieving rotation and mirror reflection equivariance in



Figure 1. Overview of the proposed Equivariant Vision Transformer. (a) The overall pipeline of the whole equivariant vision transformer. (b)-(c) The details of the EQ-Patch Embedding and the EQ-Self-Attention, respectively.

Vision Transformer. For example, rotation equivariance ensures that rotating the input leads solely to a corresponding rotation of the output, without introducing any additional, unpredictable variations. Mathematically, let  $\Psi$  denote a Vision Transformer mapping from the input feature space to the output feature space, and  $S$  be a group of rotation and mirror reflection transformations, *i.e.*,

$$S = \left\{ g(k, m) = \begin{bmatrix} (-1)^m \cos 2\pi k/t & -(-1)^m \sin 2\pi k/t \\ \sin 2\pi k/t & \cos 2\pi k/t \end{bmatrix} \right\}, \quad (1)$$

where  $k = \{0, 1, \dots, t-1\}$  and  $m \in \{0, 1\}$ . Then,  $\Psi$  is equivariant with respect to  $S$ , if for any transformation matrix  $\tilde{g} \in S$ ,

$$\Psi [\pi_{\tilde{g}}^I] (I) = \pi_{\tilde{g}}^F [\Psi] (I), \quad (2)$$

where  $I$  is an input image,  $\pi_{\tilde{g}}^I$  and  $\pi_{\tilde{g}}^F$  denote how the transformation  $\tilde{g}$  acts on input image and output features, respectively,  $[\cdot]$  denotes the composition of functions.

**Self-Attention.** We first revisit the attention mechanism in Vision Transformer. The Vision Transformer takes a visual token sequence  $z_{\ell-1} \in \mathbb{R}^{N \times d}$  from the previous layer ( $\ell-1$ th layer) as input ( $N$  is the token number and  $d$  is the hidden dimension), then projects it into the query, key, and value token sequences with three different linear projection layers, denoted as  $\mathbf{W}^q, \mathbf{W}^k, \mathbf{W}^v \in \mathbb{R}^{d \times d}$ :

$$\mathbf{q} = z_{\ell-1} \cdot \mathbf{W}^q, \mathbf{k} = z_{\ell-1} \cdot \mathbf{W}^k, \mathbf{v} = z_{\ell-1} \cdot \mathbf{W}^v. \quad (3)$$

where  $\mathbf{q}, \mathbf{k}, \mathbf{v} \in \mathbb{R}^{N \times d}$  and  $\cdot$  denotes the matrix multiplication. Then the similarity of each query  $\mathbf{q}$  and key  $\mathbf{k}$  is computed as:

$$\mathbf{A} = \text{Softmax} \left( \mathbf{q} \mathbf{k}^\top / \sqrt{d} \right), \quad (4)$$

where the attention map  $\mathbf{A}$  is an  $N \times N$  matrix with values in the range  $[0, 1]$ , and the sum of each row is normalized to 1. Then the Self-Attention reweights the value sequences  $\mathbf{v}$  according to the attention map  $\mathbf{A}$ , *i.e.*  $\mathbf{y} = \mathbf{A} \mathbf{v} \in \mathbb{R}^{N \times d}$ . The multi-head self-attention mechanism is a straightforward extension, involving parallel self-attention computations whose outputs are linearly aggregated, and is thus omitted for brevity.

**Positional Encoding.** Positional encoding in transformers is used to embed information about the position of tokens within a sequence into their input representations. In Vision Transformers, the absolute position encoding is usually set as a learnable matrix  $E_{\text{pos}}^A \in \mathbb{R}^{N \times d}$ .

In contrast to ViT [15], the Swin-Transformer [26] introduces a more dynamic approach by incorporating a relative position bias. Instead of adding position information directly to the input embeddings, the Swin-Transformer [26] injects positional information into the self-attention mechanism. Specifically, a learnable bias term  $E_{\text{pos}}^R \in \mathbb{R}^{N \times N}$  is added to the scaled dot-product attention map  $\mathbf{A}$ , *i.e.*  $\mathbf{A} + E_{\text{pos}}^R$ , modifying the similarity calculation between queries and keys. This bias is determined by the pairwise relative distance between the tokens (image patches) within a local window.

**Vision Transformers.** A standard Vision Transformer first tokenizes an input image  $\mathbf{x} \in \mathbb{R}^{C \times H \times W}$  into a sequence of embeddings. This is accomplished by a patch embedding layer, typically implemented as a 2D convolution with a kernel size and stride equal to the patch size  $s$ . This operation effectively projects each non-overlapping image patch into a  $d$ -dimensional embedding, resulting in a sequence of patch tokens. The resulting sequence  $z_0 \in \mathbb{R}^{N \times d}$  is then

processed through a stack of  $L$  transformer blocks:

$$\begin{aligned} \mathbf{z}_0 &= [\text{Transpose}(\text{Reshape}(\text{Conv2D}_s(\mathbf{x})))], \\ \mathbf{z}'_\ell &= \text{MSA}(\text{LN}(\mathbf{z}_{\ell-1})) + \mathbf{z}_{\ell-1}, & \ell = 1 \dots L \\ \mathbf{z}_\ell &= \text{MLP}(\text{LN}(\mathbf{z}'_\ell)) + \mathbf{z}'_\ell, & \ell = 1 \dots L \end{aligned} \quad (5)$$

where  $\text{Reshape}(\cdot)$  denotes reshaping the output of the  $\text{Conv2D}_s$  layer into a sequence of tokens and  $\text{Transpose}(\cdot)$  represents the reversal of dimensions. Each encoder block consists of a multi-head self-attention (MSA) module and a Multilayer Perceptron (MLP). Layer Normalization (LN) is applied before each module, and a residual connection is used after each.

### 3.2. Equivariant Patch Embedding/Self-Attention

In this section, we begin by detailing the core components of our proposed method: Equivariant Patch Embedding (EQ-PE) and Equivariant-Self-Attention (EQ-SA).

**Equivariant Patch Embedding.** In a conventional Vision Transformer, the input image  $\mathbf{x} \in \mathbb{R}^{H \times W \times c_0}$  is typically tokenized by a Patch Embedding layer to get features  $\mathbf{z}_0$ . For the proposed equivariant Vision Transformer, we will need  $\mathbf{z}_0$  to be equivariant with respect to input  $\mathbf{x}$ . We found that equivariant convolution with proper stride [50] can elegantly fulfill this requirement. Mathematically, we perform the following EQ-PE:

$$\begin{cases} \hat{\mathbf{z}}^g = D_s(\pi_A(\psi) \otimes \mathbf{x}), \forall g \in S, \\ \mathbf{z}_0 = \text{Reshape}(\hat{\mathbf{z}}), \end{cases} \quad (6)$$

where  $\hat{\mathbf{z}} \in \mathbb{R}^{\frac{H}{s} \times \frac{W}{s} \times c \times t}$  is the output feature of convolution, with  $\hat{\mathbf{z}}^g \in \mathbb{R}^{\frac{H}{s} \times \frac{W}{s} \times c}$  denotes its slice tensor indicated by  $g$  in the group dimension,  $t$  is the element number of the selected transformation group  $S$ ,  $s$  is the stride of down-sampling  $D_s$ <sup>1</sup>;  $\psi$  is a to be learned convolution kernel;  $\pi_g$  is the transformation with respect to  $g$  (e.g., rotation the with coordinate transformation matrix  $g$ );  $\otimes$  denoted a 2D convolution with input channel of  $c_0$  and output channel of  $c$ ; Reshape reshape a tensor from  $\frac{H}{s} \times \frac{W}{s} \times c \times t$  to  $N \times c \times t$ , where  $N = \frac{HW}{s^2}$ .

The above calculation is illustrated in detail in Fig. 1(b) for clarity. It should be noted that the resulting feature  $\mathbf{z}_0$  achieve by 6 is equivariant with respect to the input  $\mathbf{x}$ . When the input image is transformed, the feature  $\mathbf{z}$  moves according its corresponding image patch (patch of the receptive field), with only a predictable cyclic shift along the group channel due to the rotation or reflection of the image patch, without introducing any other unpredictable changes.

**Equivariant Self-Attention.** We take the Self-Attention layer with in put feature  $\mathbf{z} \in \mathbb{R}^{N \times c \times t}$  as example (It should be noted that in the first EQ-PE stage we have lifted the features with a additional group dimension of size  $t$ ).

<sup>1</sup>Equivariant down-sampling will be discussed in a subsequent section.

We obtain the query, key, and value by applying the following an equivariant linear layers [34] to the input  $\mathbf{z}$ :

$$\begin{aligned} \mathbf{q}^B &= \sum_{g \in S} \mathbf{z}_0^g \cdot \mathbf{W}_{B^{-1}g}^q, \forall B \in S, \\ \mathbf{k}^B &= \sum_{g \in S} \mathbf{z}_0^g \cdot \mathbf{W}_{B^{-1}g}^k, \forall B \in S, \\ \mathbf{v}^B &= \sum_{g \in S} \mathbf{z}_0^g \cdot \mathbf{W}_{B^{-1}g}^v, \forall B \in S, \end{aligned} \quad (7)$$

where  $\mathbf{q}, \mathbf{k}, \mathbf{v} \in \mathbb{R}^{N \times c \times t}$ , with  $\mathbf{q}^B, \mathbf{k}^B, \mathbf{v}^B \in \mathbb{R}^{N \times c}$  is the slice matrix indicated by  $B$  in the group dimension, respectively;  $\mathbf{W}_g^q, \mathbf{W}_g^k, \mathbf{W}_g^v \in \mathbb{R}^{c \times c}$ ,  $\forall g \in S$  denotes the learnable parameters, and  $\mathbf{z}_0^g \in \mathbb{R}^{N \times c}$  is the slice matrix of  $\mathbf{z}_0$  indicated by  $g$  in the group dimension.,

The above calculation regarding  $\mathbf{q}$  is equivalent to constructing a larger matrix  $\mathbf{W} \in \mathbb{R}^{ct \times ct}$  by tiling  $\mathbf{W}_{B^{-1}g}^q$ , and then directly multiplying it with the matrix  $\mathbf{Z} \in \mathbb{R}^{N \times ct}$  formed by  $[\mathbf{z}^{B_1}, \mathbf{z}^{B_2}, \dots, \mathbf{z}^{B_t}]$ , as shown in Fig. 1(c). It can be observed that in this process, the parameters in  $\mathbf{W}$  exhibit clear cyclic shifting and sharing patterns. It can be proven that the linear operation performed in this manner is equivariant [34]. The same patterns holds for  $\mathbf{k}$  and  $\mathbf{v}$  too.

After obtaining query, key, and value, we compute the attention map  $\mathbf{A}$  and the final output  $\mathbf{z}_1$

$$\mathbf{A} = \text{Softmax} \left( \mathbf{Q} \cdot \mathbf{K}^\top / \sqrt{ct} \right), \mathbf{z}_1 = \mathbf{A} \cdot \mathbf{V}, \quad (8)$$

where  $\mathbf{K}, \mathbf{Q}, \mathbf{V} \in \mathbb{R}^{N \times ct}$  are matrixes reshaped from  $\mathbf{q}, \mathbf{k}, \mathbf{v} \in \mathbb{R}^{N \times c \times t}$ .

The above calculation is illustrated in detail in Fig. 1(c) for clarity. A similar process can be intuitively deduced from the construction of equivariant Multi-Head Self-Attention.

### 3.3. Equivariant Positional Encoding

Vision Transformers typically incorporate positional encodings to model spatial relationships between image patches. These are commonly implemented in two forms: absolute position encoding, which assigns a unique embedding to each patch, and relative position encoding, which explicitly models pairwise spatial offsets between patches.

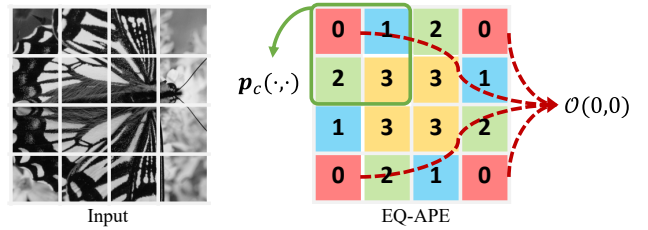


Figure 2. The visualization of the input and the proposed Equivariant APE for  $C_4$  group. For EQ-APE, different numbers represent different orbits. And  $\mathbf{p}_c(\cdot, \cdot)$  denote the canonical representations

**Equivariant Absolute Positional Encoding.** Let the input image be discretized into a grid of  $N \times N$  patches. The position of any patch is indexed by its 2D coordinates  $\mathbf{p} = (i, j)$ , where  $i, j \in \{0, \dots, N-1\}$ . Let’s take the cyclic group  $C_4$  of 90-degree rotations as an example<sup>2</sup>. The action of this group on a position  $\mathbf{p}$  generates a set of equivalent positions, known as the orbit  $\mathcal{O}(\mathbf{p})$ <sup>3</sup>. For any position  $(i, j)$ :

$$\mathcal{O}(i, j) = \{(i, j), (j, N-1-i), (N-1-i, N-1-j), (N-1-j, i)\}, \quad (9)$$

and in Figure 2, we visualize the orbit of the position  $(0, 0)$ .

To ensure all positions within an orbit share an identical embedding, we first map each position  $\mathbf{p}$  to a canonical representative  $\mathbf{p}_c$  of its orbit. Specifically, we define the canonical representation, shown in Figure 2, as the lexicographically smallest element within the orbit:

$$\mathbf{p}_c(i, j) = \min_{\text{lex}} \mathcal{O}(i, j), \quad (10)$$

where  $\min_{\text{lex}}$  denotes the selection of the element that is smallest in lexicographical order. For two-dimensional coordinates, a pair  $(i_1, j_1)$  is considered lexicographically smaller than  $(i_2, j_2)$  if  $i_1 < i_2$ , or if  $i_1 = i_2$  and  $j_1 < j_2$ .

For a position  $p = (i, j)$  with its orbit representative  $p_c(i, j)$ , given that the absolute positional encoding  $\text{APE}(\cdot)$  is assigned to  $p_c$ , then all elements within the group orbit of this coordinate share the same APE. Specifically, our  $C_4$ -invariant absolute position encoding can be formally expressed as:

$$\text{PE}_{C_4}(i, j) = \text{APE}(\mathbf{p}_c(i, j)). \quad (11)$$

This construction guarantees that for any rotation  $g \in C_4$ , the encoding remains invariant, i.e.,  $\text{PE}_{C_4}(g(\mathbf{p})) = \text{PE}_{C_4}(\mathbf{p})$ , thereby providing the model with a consistent representation of spatial location regardless of the input’s orientation. For the construction of the APE for the mirror transformation group, see the supplementary materials.

**Equivariant Relative Position Encoding.** A core objective of relative position encoding (RPE) is to model intrinsic spatial relationships between token pairs, independent of their global pose. However, standard RPEs, typically based on displacement vectors, are sensitive to rotations and reflections, and fail to recognize that transformed pairs remain geometrically congruent. To address this, we introduce an RPE formulation based on the dihedral group  $D_4$ , which captures the full set of eight square symmetries: four rotations ( $0^\circ, 90^\circ, 180^\circ, 270^\circ$ ) and four reflections (horizontal, vertical, and two diagonals). Our method ensures invariance under  $D_4$  by assigning identical positional encodings

<sup>2</sup>The set of 90-degree rotations is known in mathematics as the cyclic group  $C_4$ , contains four distinct rotation orientations:  $0^\circ, 90^\circ, 180^\circ$ , and  $270^\circ$ .

<sup>3</sup>The orbit of an element  $x$  under the action of a group  $S$  is the set of all elements that can be reached by applying the transformations of  $S$  to  $x$ .

to any two patch pairs that are equivalent under these transformations.

To achieve this, we generalize the concept of canonical representation to the group  $D_4$ . We define the orbit of the pair  $(\mathbf{p}_i, \mathbf{p}_j)$  as the set of all pairs reachable by applying the same group element  $g \in D_4$  to both points:

$$\mathcal{O}_{D_4}(\mathbf{p}_i, \mathbf{p}_j) = \{(g(\mathbf{p}_i), g(\mathbf{p}_j)) \mid g \in D_4\}. \quad (12)$$

Within this orbit, which contains all geometrically equivalent configurations of the point pair, we select a **canonical representative**. This representative, denoted  $(\mathbf{p}_{ic}, \mathbf{p}_{jc})$ , is chosen as the lexicographically smallest element in the orbit, where the comparison is performed on the flattened 4-tuple representation  $(i_1, j_1, i_2, j_2)$ :

$$(\mathbf{p}_{ic}, \mathbf{p}_{jc}) = \min_{\text{lex}} \mathcal{O}_{D_4}(\mathbf{p}_i, \mathbf{p}_j). \quad (13)$$

Finally, our  $D_4$ -invariant relative position encoding is defined by applying a base RPE function (such as a learnable embedding) to the displacement vector of this canonical pair:

$$\text{PE}_{D_4}^{\text{rel}}(\mathbf{p}_i, \mathbf{p}_j) = \text{RPE}(\mathbf{p}_{jc} - \mathbf{p}_{ic}). \quad (14)$$

This construction maps any point pair along with its rotated or reflected counterparts to the same canonical displacement vector, effectively normalizing relative orientation prior to encoding. As a result, the self-attention mechanism gains true geometric invariance, enabling the model to focus on fundamental spatial relationships and improving both generalization capability and data efficiency.

### 3.4. Equivariant Down/Up-Sampling

To capture multi-scale visual features, recent Vision Transformers often employ down-sampling at various stages. This includes initial patch embedding via strided convolution, as well as subsequent down-sampling layers like patch merging, to reduce spatial resolution. Meanwhile, certain tasks utilize up-sampling layers, such as PixelShuffle, to increase resolution. However, these conventional down-sampling and up-sampling operations inherently break group equivariance. Therefore, designing equivariant resampling layers is a necessary step toward building fully equivariant Vision Transformers.

**Equivariant down-sampling.** Standard down-sampling operations are not equivariant as they impose a fixed sampling lattice on the feature space[8, 50]. Let  $F \in \mathbb{R}^{H \times W \times (n \times t)}$  be a feature map in a  $\mathcal{G}$ -equivariant network layer, and  $\mathcal{G} = \{1, \dots, t\}$ . we have

$$F = \left[ \underbrace{F_1^1, \dots, F_t^1, \dots, F_1^n, \dots, F_t^n}_{|\mathcal{G}|=t} \right] \quad (15)$$

Our method is to construct a  $\mathcal{G}$ -equivariant down-sampling operator by ensuring the sampling grid effectively co-transforms along with the features. Firstly, we disentangle  $F$  into  $t$  sub-maps  $\{F_g\}_{g \in \mathcal{G}}$ , where each  $F_g \in \mathbb{R}^{H \times W \times n}$  consists of the all channels corresponding to the element  $g \in \mathcal{G}$ . The key insight is to map each feature map  $F_g$  back to a canonical one, then apply the standard down-sampling, and finally transform the result back to its original group index.

Formally, for any group element  $g \in \mathcal{G}$ , the corresponding output feature map  $\tilde{F}_g$  is computed as:

$$\tilde{F}_g = [\pi(g) \circ \text{Down}_s \circ \pi(g^{-1})] (F_g), \quad \forall g \in \mathcal{G}. \quad (16)$$

where  $\pi(\cdot)$  denotes the group transformation operator,  $\text{Down}_s$  is a  $s$ -stride down-sampling operator, and  $\circ$  represents function composition. And all processed sub-maps  $\{\tilde{F}_g\}_{g \in \mathcal{G}}$  are re-interleaved to construct the final output  $F_{\text{out}} \in \mathbb{R}^{rH \times rW \times (n \times t)}$ , like Eq.(15), which restores the standard  $\mathcal{G}$ -equivariant channel ordering. Specific examples and proofs of equivariance are provided in the supplementary materials.

**Equivariant Up-Sampling (Pixel-Shuffle).** Standard up-sampling layers, such as Pixel-Shuffle [39], are not group-equivariant by nature, as their fixed spatial reshaping pattern disrupts the channel-wise encoding of group transformations. To overcome this limitation, we introduce an Equivariant Pixel-Shuffle (E-PS) layer that preserves the group structure of features throughout the up-sampling process.

Let  $F \in \mathbb{R}^{H \times W \times (r^2 n \times t)}$  be the input feature map for an  $r \times$  up-sampling. Our method also begins by disentangling  $F$  into  $t$  sub-maps  $\{F_g\}_{g \in \mathcal{G}}$ , where each  $F_g \in \mathbb{R}^{H \times W \times (r^2 n)}$ . To apply a standard up-sampling operation isotropically, we formulate a composite function that first maps each  $F_g$  to a canonical one, applies Pixel-Shuffle, and then transforms the result back to its original one. This entire sequence yields the upsampled and correctly re-oriented sub-map  $\tilde{F}_g$ :

$$\tilde{F}_g = [\pi(g) \circ \text{PS}_r \circ \pi(g^{-1})] (F_g), \quad \forall g \in \mathcal{G} \quad (17)$$

where  $\pi(\cdot)$  denotes the group transformation,  $\text{PS}_r(\cdot)$  is the standard Pixel-Shuffle operator that reshapes a tensor of  $r^2 C$  channels to  $C$  channels with  $r \times$  larger spatial dimensions, and  $\circ$  represents function composition.

Finally, all processed sub-maps  $\{\tilde{F}_g\}_{g \in \mathcal{G}}$  are re-interleaved to construct the final output  $F_{\text{out}} \in \mathbb{R}^{rH \times rW \times (n \times t)}$ , like Eq.(15), which restores the standard  $\mathcal{G}$ -equivariant channel ordering. Specific examples and proofs of equivariance are provided in the supplementary materials.

### 3.5. EQ-LayerNorm.

A standard Layer Normalization (LN) layer includes a learnable affine transformation with scaling parameters  $\gamma$

and shifting parameters  $\beta$ , both in  $\mathbb{R}^C$ . Applying this naively would assign an independent parameter to each channel for equivariant features  $z \in \mathbb{R}^{N \times C}$ , thus breaking the structural dependency within each group-related block of channels and violating equivariance.

To enforce equivariance, we introduce a Group Equivariant Layer Normalization (EQ-LN) layer that employs parameter sharing. After the standard normalization step, we apply a shared affine transformation. Specifically, we define a reduced set of learnable parameters  $\gamma, \beta \in \mathbb{R}^C$ . Specifically,  $\gamma$  and  $\beta$  have a weight-sharing along the group dimension. This ensures that all features belonging to the same group orbit are transformed by the exact same learnable parameters. Consequently, our EQ-LN layer commutes with the group action on the channel axis, rigorously preserving the network's group equivariance. More details can be found in the supplementary materials.

### 3.6. Theoretical Analysis.

In this section, we provide a rigorous theoretical analysis to establish the formal properties of our proposed architecture. Our analysis is twofold: first, we prove that our model achieves exact group equivariance to rotations and reflections (Theorem 1). Second, we derive a novel generalization error bound (Theorem 2) that quantifies the benefits of this equivariant design, formally linking the imposed symmetry to improved sample complexity.

**Theorem 1.** *Let  $\Phi_{\text{eq}}(\cdot)$  denotes an equivariant transformer including  $L$ -layer equivariant Self-Attention defined in Eq.(8). For an image  $\mathbf{x}$  with size  $H \times W \times c_0$ , then the following result is satisfied for  $\forall \tilde{g} \in S$ :*

$$\Phi_{\text{eq}}[\pi_{\tilde{g}}](\mathbf{x}) = \pi_{\tilde{g}}[\Phi_{\text{eq}}](\mathbf{x}), \quad (18)$$

where  $\pi_{\tilde{g}}$  is a group transformation on the feature map and  $[\cdot]$  denotes the composition of functions.

Theorem 1 shows that the proposed equivariant Vision Transformer is theoretically exact group equivariant with the rotation and mirror reflection. The proof can be found in the supplementary materials.

**Theorem 2.** *For an image  $\mathbf{x}$  with size  $H \times W \times c_0$ , and a equivariant transformer  $\Phi_{\text{eq}}(\cdot)$  including  $L$ -layer equivariant self-attention, whose embedding dimension of the  $i^{\text{th}}$  layer is  $d_i$ , for the group  $S$ ,  $|S| = t$ , and activation function is set as GELU. If the latent continuous function of the  $c^{\text{th}}$  channel of  $\mathbf{x}$  denoted as  $r_c : \mathbb{R}^2 \rightarrow \mathbb{R}$ , the weight of patch embedding as  $W_0$ , and the  $i^{\text{th}}$  linear layer weight of query, key, and value as  $W_{(l)}^Q$ ,  $W_{(l)}^K$ , and  $W_{(l)}^V$ . The following conditions are satisfied:*

$$\begin{aligned} |r_c(x)| &\leq F_0, \|W_0\|_{\text{op}} \leq \rho_0 \\ \|W_{(l)}^Q\|_{\text{op}} &\leq \rho_Q^{(l)}, \|W_{(l)}^K\|_{\text{op}} \leq \rho_K^{(l)}, \|W_{(l)}^V\|_{\text{op}} \leq \rho_V^{(l)}, \end{aligned} \quad (19)$$

Then we have:

$$GE(\Phi_{eq}) \leq \frac{C}{\sqrt{n}} \frac{1}{t^{1/2}} + O\left(\sqrt{\frac{\log(1/\delta)}{n}}\right), \quad (20)$$

where  $C$  is determined by embedding dimensions  $d$ , the norm of the each linear layer, and the smoothness bounds of the input function.

Theorem 2 derives the generalization error bound of our proposed Vision Transformer, establishing a formal upper bound under the action of the group Vision Transformers. This is essentially because isovariant networks introduce parameter sharing; fewer parameters mean lower model complexity, thus the network generalization error can be expected to be reduced. A precise derivation is provided in the supplementary materials.

## 4. Experiments

In this section, we integrate the proposed equivariant modules into command used ViT and Swin Transformer architectures, constructing strictly equivariant networks for image classification, object detection, and semantic segmentation. The modules are further extended to SwinIR for low-level vision tasks, including image super-resolution and video arbitrary-scale super-resolution.

### 4.1. Image Classification

**Datasets and Training Details.** For image classification, the ImageNet-1K [20] dataset contains 1.28M training Images and 50K validation images with a total of 1,000 classes. *miniImageNet* includes 50K training images and 10K validation images across 100 categories. Specifically, images are trained and evaluated in  $224 \times 224$  size for image classification. The top-1 and top-5 accuracy on the validation set is adopted as the evaluation metrics. For ViT, we adopt the republic github repository<sup>4</sup> to conduct all experiments. For Swin-Transformer, we follow the official release code to conduct all experiments. The training setting follows the image classification experiments are conducted on ImageNet-1K [20] and *miniImageNet* [43] datasets. In addition, We denote the variants of baseline models enhanced with rotation equivariance and reflection equivariance using the suffixes -EQ and -EQ-R, respectively.

**Quantitative Results.** As shown in Table 1, our method demonstrates notable improvements across various Vision Transformer architectures on the ImageNet-1K and *miniImageNet* datasets. These quantitative results validate that our proposed equivariant methods effectively enhance classification accuracy. It is a well-documented observation that ViT, when trained from scratch without large-scale pre-training, often struggle to converge on smaller

Table 1. Classification performance comparison on ImageNet-1K and *miniImageNet*. All images are of size  $224 \times 224$ . T, S, and B denote the tiny, small, and base scales, respectively. And the suffixes -EQ and -EQ-R denote rotation equivariance and mirror reflection equivariance, respectively.

Model	Image Size	Param.	Top-1 (%)	Top-5 (%)
<b>(a) ImageNet-1K</b>				
RegNetY-4G [33]	$224^2$	21M	79.23	94.65
RegNetY-8G [33]	$224^2$	39M	79.88	94.83
RegNetY-16G [33]	$224^2$	84M	79.88	94.83
DeiT-T[41]	$224^2$	6M	72.20	91.10
DeiT-S[41]	$224^2$	22M	79.90	95.00
DeiT-B[41]	$224^2$	86M	81.80	95.60
ViT-T [15]	$224^2$	6M	74.28	91.86
ViT-T-EQ	$224^2$	8M	74.41	91.88
ViT-T-EQ-R	$224^2$	7M	74.57	91.90
ViT-S [15]	$224^2$	22M	78.23	93.87
ViT-S-EQ-R	$224^2$	17M	78.69	94.24
ViT-B [15]	$224^2$	87M	77.18	93.11
ViT-B-EQ-R	$224^2$	38M	80.28	94.91
Swin-T	$224^2$	28M	80.99	95.41
Swin-T-EQ	$224^2$	28M	82.07	95.92
Swin-T-EQ-R	$224^2$	31M	81.10	95.54
<b>(b) miniImageNet</b>				
DeiT-S [41]	$224^2$	22M	70.83	89.74
DeiT-B [41]	$224^2$	86M	72.43	90.14
XCiT-S24 [3]	$224^2$	26M	85.79	96.31
XCiT-M24 [3]	$224^2$	84M	86.80	96.38
Swin-T [26]	$224^2$	28M	87.06	97.46
Swin-T-EQ-R	$224^2$	14M	87.08	97.52

datasets. Consequently, we do not report results for ViT on the *miniImageNet* benchmark.

**Object Detection and Semantic Segmentation.** For object detection, experiments are conducted on COCO 2017, which contains 118K training, 5K validation, and 20K test-dev images. For semantic segmentation, the ADE20K [60] dataset cover a broad range of 150 semantic categories. It's 20K for training, 2K for validation, and another 3K for testing. Using Swin-T as our visual encoder, we integrate it with Mask R-CNN [17] for detection and UPerNet [51] for segmentation. Compared to the baseline, our equivariant model demonstrates notable performance gains. On ADE20K, we improve the semantic segmentation mIoU from 44.51 to **44.86**. For object detection on COCO, our approach elevates the box mAP from 43.7 to **45.4** (+1.7) and the mask mAP from 39.8 to **41.2** (+1.4).

### 4.2. Image Super-Resolution

**Datasets and Training Details.** Following the setup in previous works [25, 57], we employ DIV2K [2] to train classic SR models. Then we use Urban100 [19], BSD100 [28], Set14 [56], Set5 [4], and Manga109 [29] to evaluate the effectiveness of different SR methods. All comparison meth-

<sup>4</sup><https://github.com/huggingface/pytorch-image-models>

Table 2. Quantitative comparison (average PSNR/SSIM) for classical image SR on benchmark datasets.

Method	Scale	Para.	Urban100		BSD100		Set14		Set5		Manga100	
			PSNR	SSIM								
RCAN [58]	$\times 2$	15.4M	33.34	0.9384	32.41	0.9027	34.12	0.9216	38.27	0.9614	39.44	0.9786
SAN [12]	$\times 2$	15.7M	33.10	0.9370	32.42	0.9028	34.07	0.9213	38.31	0.9620	39.32	0.9792
IGNN [61]	$\times 2$	-	33.23	0.9383	32.41	0.9025	34.07	0.9217	38.24	0.9613	39.35	0.9786
HAN [32]	$\times 2$	16.1M	33.35	0.9385	32.41	0.9027	34.16	0.9217	38.27	0.9614	39.46	0.9785
NLSA [30]	$\times 2$	-	33.42	0.9394	32.43	0.9027	34.08	0.9231	38.34	0.9618	39.59	0.9789
SwinIR [25]	$\times 2$	11.8M	33.44	0.9399	32.45	0.9030	<b>34.16</b>	<b>0.9232</b>	38.32	0.9619	39.57	<b>0.9789</b>
SwinIR-EQ	$\times 2$	5.2M	<b>33.54</b>	<b>0.9409</b>	<b>32.46</b>	<b>0.9032</b>	34.10	0.9227	<b>38.38</b>	<b>0.9620</b>	<b>39.59</b>	0.9788

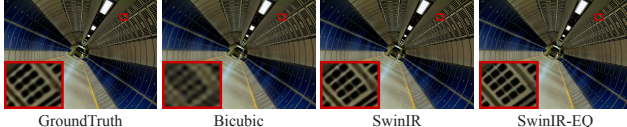


Figure 3. The visual comparison of the 4 times super resolution results from various methods on img078 of the Urban100.

ods were trained in the same way as the original method, and the proposed method was trained using the same strategy as the baseline SwinIR [25]. In image super-resolution, we consider cases of rotational equivalence.

**Quantitative Results.** The results in Table 2 show that our proposed SwinIR-EQ achieves a compelling trade-off between performance and parameter efficiency. Compared to its powerful baseline, SwinIR-EQ demonstrates clear performance gains across most benchmark datasets for  $\times 2$  super-resolution. For instance, on the structurally rich Urban100 dataset, our method improves the PSNR for both scaling factors. Remarkably, these accuracy gains are achieved with a significantly more compact model. The SwinIR-EQ ( $\times 2$ ) utilizes only **5.2M** parameters, which is less than half the size of SwinIR (11.8M) and a small fraction of larger models like RCAN (15.4M). This dual improvement strongly validates our core hypothesis: by embedding rotation equivariance as an inductive bias, the model learns a more powerful and generalizable representation, reducing the need for a large parameter count while delivering superior restoration quality. The visual results are shown in Figure 3.

Ablation experiments and further experimental results can be found in the supplementary materials.

### 4.3. Video Arbitrary Super-Resolution

**Datasets and Training Details.** All methods trained on the REDS dataset [31], which comprises 240 videos of resolution  $720 \times 1,280$  captured by GoPro. Each video consists of 100 HR frames. Following the settings in [7, 37], we generate LR frames using the bicubic degradation model, with randomly sampled scaling factors from a uniform distribution  $\mathcal{U}[1, 4]$ . We test on the validation set of REDS comprising 30 videos. We train to follow the original method. Here, we consider cases of rotational equivalence.

Table 3. Quantitative comparison with state-of-the-art methods on the REDS validation set (PSNR $\uparrow$  / SSIM $\uparrow$ ). The best results are highlighted in boldface.

Method	$\times 2$	$\times 3$	$\times 4$
Bicubic	31.51/0.911	26.82/0.788	24.92/0.713
EDVR [46]	36.03/0.961	32.59/0.904	30.24/0.853
ArbSR [44]	34.48/0.942	30.51/0.862	28.38/0.799
EQSR [47]	34.71/0.943	30.71/0.867	28.75/0.804
RDN [59] + LTE [23]	34.63/0.942	30.64/0.865	28.65/0.801
RDN-EQ + LTE-EQ	<b>34.73/0.943</b>	30.68/0.867	28.68/0.802
SwinIR [25] + LTE [23]	34.73/0.943	30.73/0.866	28.75/0.804
SwinIR-EQ + LTE-EQ	34.79/0.945	30.77/0.868	28.78/0.804

**Quantitative Results.** To further demonstrate the versatility of our approach, we apply our method to the task of video arbitrary super-resolution. As shown in Table 3, our equivariant models consistently outperform their non-equivariant counterparts across all scaling factors ( $\times 2, \times 3, \times 4$ ). These results clearly indicate that embedding equivariance is an effective strategy that can further enhance the quality of video restoration.

## 5. Conclusion

In this work, we present a comprehensive framework to instill group equivariance into Vision Transformers by systematically redesigning each of its core components. Our approach constructs a holistic equivariant architecture, beginning with an equivariant patch embedding and extending to the self-attention mechanism through equivariant linear projections. Crucially, we introduce novel equivariant positional encodings by mapping absolute and relative coordinates to canonical representatives of their symmetry orbits, and preserve architectural integrity through equivariant resampling layers and group-aware normalization. This principled design culminates in a model that is not only provably equivariant, as supported by our theoretical analysis, but also empirically demonstrates consistent improvements in performance and data efficiency. The successful application of our framework to the Swin Transformer underscores its versatility and practical value, paving the way for a new class of Vision Transformers that possess a more fundamental and robust understanding of the visual world.

## References

[1] Pulkit Agrawal, Joao Carreira, and Jitendra Malik. Learning to see by moving. In *Proceedings of the IEEE international conference on computer vision*, pages 37–45, 2015. [1](#), [2](#)

[2] Eirikur Agustsson and Radu Timofte. Ntire 2017 challenge on single image super-resolution: Dataset and study. In *Proceedings of the IEEE conference on computer vision and pattern recognition workshops*, pages 126–135, 2017. [7](#)

[3] Alaaeldin Ali, Hugo Touvron, Mathilde Caron, Piotr Bojanowski, Matthijs Douze, Armand Joulin, Ivan Laptev, Natalia Neverova, Gabriel Synnaeve, Jakob Verbeek, et al. Xcit: Cross-covariance image transformers. *Advances in neural information processing systems*, 34:20014–20027, 2021. [7](#)

[4] Marco Bevilacqua, Aline Roumy, Christine Guillemot, and Marie Line Alberi-Morel. Low-complexity single-image super-resolution based on nonnegative neighbor embedding. 2012. [7](#)

[5] Georg Bökman, David Nordström, and Fredrik Kahl. Flopping for flops: Leveraging equivariance for computational efficiency. *arXiv preprint arXiv:2502.05169*, 2025. [2](#)

[6] Nicolas Carion, Francisco Massa, Gabriel Synnaeve, Nicolas Usunier, Alexander Kirillov, and Sergey Zagoruyko. End-to-end object detection with transformers. In *European conference on computer vision*, pages 213–229. Springer, 2020. [2](#)

[7] Yi-Hsin Chen, Si-Cun Chen, Yen-Yu Lin, and Wen-Hsiao Peng. Motif: Learning motion trajectories with local implicit neural functions for continuous space-time video super-resolution. In *Proceedings of the IEEE/CVF international conference on computer vision*, pages 23131–23141, 2023. [8](#)

[8] Taco Cohen and Max Welling. Group equivariant convolutional networks. In *International conference on machine learning*, pages 2990–2999. PMLR, 2016. [1](#), [2](#), [5](#)

[9] Taco S Cohen and Max Welling. Steerable cnns. *arXiv preprint arXiv:1612.08498*, 2016. [1](#)

[10] Taco S Cohen, Mario Geiger, and Maurice Weiler. A general theory of equivariant cnns on homogeneous spaces. *Advances in neural information processing systems*, 32, 2019. [2](#)

[11] Colin Conwell, Jacob S Prince, Kendrick N Kay, George A Alvarez, and Talia Konkle. A large-scale examination of inductive biases shaping high-level visual representation in brains and machines. *Nature communications*, 15(1):9383, 2024. [1](#)

[12] Tao Dai, Jianrui Cai, Yongbing Zhang, Shu-Tao Xia, and Lei Zhang. Second-order attention network for single image super-resolution. In *Proceedings of the IEEE/CVF conference on computer vision and pattern recognition*, pages 11065–11074, 2019. [8](#)

[13] Sander Dieleman, Jeffrey De Fauw, and Koray Kavukcuoglu. Exploiting cyclic symmetry in convolutional neural networks. In *International conference on machine learning*, pages 1889–1898. PMLR, 2016. [1](#), [2](#)

[14] Peijian Ding, Davit Soselia, Thomas Armstrong, Jiahao Su, and Furong Huang. Reviving shift equivariance in vision transformers. *arXiv preprint arXiv:2306.07470*, 2023. [1](#), [2](#)

[15] Alexey Dosovitskiy. An image is worth 16x16 words: Transformers for image recognition at scale. *arXiv preprint arXiv:2010.11929*, 2020. [1](#), [2](#), [3](#), [7](#)

[16] Haoqi Fan, Bo Xiong, Karttikeya Mangalam, Yanghao Li, Zhicheng Yan, Jitendra Malik, and Christoph Feichtenhofer. Multiscale vision transformers. In *Proceedings of the IEEE/CVF international conference on computer vision*, pages 6824–6835, 2021. [1](#), [2](#)

[17] Kaiming He, Georgia Gkioxari, Piotr Dollár, and Ross Girshick. Mask r-cnn. In *Proceedings of the IEEE international conference on computer vision*, pages 2961–2969, 2017. [7](#)

[18] Lingshen He, Yuxuan Chen, Yiming Dong, Yisen Wang, Zhouchen Lin, et al. Efficient equivariant network. *Advances in Neural Information Processing Systems*, 34:5290–5302, 2021. [1](#), [2](#)

[19] Jia-Bin Huang, Abhishek Singh, and Narendra Ahuja. Single image super-resolution from transformed self-exemplars. In *Proceedings of the IEEE conference on computer vision and pattern recognition*, pages 5197–5206, 2015. [7](#)

[20] Alex Krizhevsky, Ilya Sutskever, and Geoffrey E Hinton. Imagenet classification with deep convolutional neural networks. *Advances in neural information processing systems*, 25, 2012. [2](#), [7](#)

[21] Soumyabrata Kundu and Risi Kondor. Steerable transformers for volumetric data. *arXiv preprint arXiv:2405.15932*, 2024. [1](#), [2](#)

[22] Dmitry Laptev, Nikolay Savinov, Joachim M Buhmann, and Marc Pollefeys. Ti-pooling: transformation-invariant pooling for feature learning in convolutional neural networks. In *Proceedings of the IEEE conference on computer vision and pattern recognition*, pages 289–297, 2016. [2](#)

[23] Jaewon Lee and Kyong Hwan Jin. Local texture estimator for implicit representation function. In *Proceedings of the IEEE/CVF conference on computer vision and pattern recognition*, pages 1929–1938, 2022. [8](#)

[24] Yanghao Li, Chao-Yuan Wu, Haoqi Fan, Karttikeya Mangalam, Bo Xiong, Jitendra Malik, and Christoph Feichtenhofer. Mvitv2: Improved multiscale vision transformers for classification and detection. In *Proceedings of the IEEE/CVF conference on computer vision and pattern recognition*, pages 4804–4814, 2022. [2](#)

[25] Jingyun Liang, Jie Zhang Cao, Guolei Sun, Kai Zhang, Luc Van Gool, and Radu Timofte. Swinir: Image restoration using swin transformer. In *Proceedings of the IEEE/CVF international conference on computer vision*, pages 1833–1844, 2021. [2](#), [7](#), [8](#)

[26] Ze Liu, Yutong Lin, Yue Cao, Han Hu, Yixuan Wei, Zheng Zhang, Stephen Lin, and Baining Guo. Swin transformer: Hierarchical vision transformer using shifted windows. In *Proceedings of the IEEE/CVF international conference on computer vision*, pages 10012–10022, 2021. [1](#), [2](#), [3](#), [7](#)

[27] Ze Liu, Han Hu, Yutong Lin, Zhuliang Yao, Zhenda Xie, Yixuan Wei, Jia Ning, Yue Cao, Zheng Zhang, Li Dong, et al. Swin transformer v2: Scaling up capacity and resolution. In

*Proceedings of the IEEE/CVF conference on computer vision and pattern recognition*, pages 12009–12019, 2022. 2

[28] David Martin, Charless Fowlkes, Doron Tal, and Jitendra Malik. A database of human segmented natural images and its application to evaluating segmentation algorithms and measuring ecological statistics. In *Proceedings eighth IEEE international conference on computer vision. ICCV 2001*, pages 416–423. IEEE, 2001. 7

[29] Yusuke Matsui, Kota Ito, Yuji Aramaki, Azuma Fujimoto, Toru Ogawa, Toshihiko Yamasaki, and Kiyoharu Aizawa. Sketch-based manga retrieval using manga109 dataset. *Multimedia tools and applications*, 76(20):21811–21838, 2017. 7

[30] Yiqun Mei, Yuchen Fan, and Yuqian Zhou. Image super-resolution with non-local sparse attention. In *Proceedings of the IEEE/CVF conference on computer vision and pattern recognition*, pages 3517–3526, 2021. 8

[31] Seungjun Nah, Sungyong Baik, Seokil Hong, Gyeongsik Moon, Sanghyun Son, Radu Timofte, and Kyoung Mu Lee. Ntire 2019 challenge on video deblurring and super-resolution: Dataset and study. In *Proceedings of the IEEE/CVF conference on computer vision and pattern recognition workshops*, pages 0–0, 2019. 8

[32] Ben Niu, Weilei Wen, Wenqi Ren, Xiangde Zhang, Lianping Yang, Shuzhen Wang, Kaihao Zhang, Xiaochun Cao, and Haifeng Shen. Single image super-resolution via a holistic attention network. In *European conference on computer vision*, pages 191–207. Springer, 2020. 8

[33] Ilija Radosavovic, Raj Prateek Kosaraju, Ross Girshick, Kaiming He, and Piotr Dollár. Designing network design spaces. In *Proceedings of the IEEE/CVF conference on computer vision and pattern recognition*, pages 10428–10436, 2020. 7

[34] Siamak Ravanbakhsh. Universal equivariant multilayer perceptrons. In *International Conference on Machine Learning*, pages 7996–8006. PMLR, 2020. 2, 4

[35] Renan A Rojas-Gomez, Teck-Yian Lim, Minh N Do, and Raymond A Yeh. Making vision transformers truly shift-equivariant. In *Proceedings of the IEEE/CVF Conference on Computer Vision and Pattern Recognition*, pages 5568–5577, 2024. 1, 2

[36] David W Romero and Jean-Baptiste Cordonnier. Group equivariant stand-alone self-attention for vision. *arXiv preprint arXiv:2010.00977*, 2020. 1, 2

[37] Wei Shang, Dongwei Ren, Wanying Zhang, Yuming Fang, Wangmeng Zuo, and Kede Ma. Arbitrary-scale video super-resolution with structural and textural priors. In *European Conference on Computer Vision*, pages 73–90. Springer, 2024. 8

[38] Zhengyang Shen, Lingshen He, Zhouchen Lin, and Jinwen Ma. Pdo-econvs: Partial differential operator based equivariant convolutions. In *International Conference on Machine Learning*, pages 8697–8706. PMLR, 2020. 1, 2

[39] Wenzhe Shi, Jose Caballero, Ferenc Huszár, Johannes Totz, Andrew P Aitken, Rob Bishop, Daniel Rueckert, and Zehan Wang. Real-time single image and video super-resolution using an efficient sub-pixel convolutional neural network. In *Proceedings of the IEEE conference on computer vision and pattern recognition*, pages 1874–1883, 2016. 6

[40] Patrice Y Simard, David Steinkraus, John C Platt, et al. Best practices for convolutional neural networks applied to visual document analysis. In *Icdar*. Edinburgh, 2003. 2

[41] Hugo Touvron, Matthieu Cord, Matthijs Douze, Francisco Massa, Alexandre Sablayrolles, and Hervé Jégou. Training data-efficient image transformers & distillation through attention. In *International conference on machine learning*, pages 10347–10357. PMLR, 2021. 1, 7

[42] Ashish Vaswani, Noam Shazeer, Niki Parmar, Jakob Uszkoreit, Llion Jones, Aidan N Gomez, Łukasz Kaiser, and Illia Polosukhin. Attention is all you need. *Advances in neural information processing systems*, 30, 2017. 2

[43] Oriol Vinyals, Charles Blundell, Timothy Lillicrap, Daan Wierstra, et al. Matching networks for one shot learning. *Advances in neural information processing systems*, 29, 2016. 7

[44] Longguang Wang, Yingqian Wang, Zaiping Lin, Jungang Yang, Wei An, and Yulan Guo. Learning a single network for scale-arbitrary super-resolution. In *Proceedings of the IEEE/CVF international conference on computer vision*, pages 4801–4810, 2021. 8

[45] Wenhui Wang, Enze Xie, Xiang Li, Deng-Ping Fan, Kaitao Song, Ding Liang, Tong Lu, Ping Luo, and Ling Shao. Pyramid vision transformer: A versatile backbone for dense prediction without convolutions. In *Proceedings of the IEEE/CVF international conference on computer vision*, pages 568–578, 2021. 2

[46] Xintao Wang, Kelvin CK Chan, Ke Yu, Chao Dong, and Chen Change Loy. Edvr: Video restoration with enhanced deformable convolutional networks. In *Proceedings of the IEEE/CVF conference on computer vision and pattern recognition workshops*, pages 0–0, 2019. 8

[47] Xiaohang Wang, Xuanhong Chen, Bingbing Ni, Hang Wang, Zhengyan Tong, and Yutian Liu. Deep arbitrary-scale image super-resolution via scale-equivariance pursuit. In *Proceedings of the IEEE/CVF Conference on Computer Vision and Pattern Recognition*, pages 1786–1795, 2023. 8

[48] Maurice Weiler and Gabriele Cesa. General E(2)-Equivariant Steerable CNNs. In *Conference on Neural Information Processing Systems (NeurIPS)*, 2019. 2

[49] Haiping Wu, Bin Xiao, Noel Codella, Mengchen Liu, Xiyang Dai, Lu Yuan, and Lei Zhang. Cvt: Introducing convolutions to vision transformers. In *Proceedings of the IEEE/CVF international conference on computer vision*, pages 22–31, 2021. 2

[50] Xiuyu Wu, Xinhao Wang, Xiubin Zhu, Lan Yang, Jiyuan Liu, and Xingchen Hu. Measuring the impact of rotation equivariance on aerial object detection. In *Proceedings of the IEEE/CVF International Conference on Computer Vision*, pages 7329–7339, 2025. 4, 5

[51] Tete Xiao, Yingcheng Liu, Bolei Zhou, Yuning Jiang, and Jian Sun. Unified perceptual parsing for scene understanding. In *Proceedings of the European conference on computer vision (ECCV)*, pages 418–434, 2018. 7

[52] Enze Xie, Wenhui Wang, Zhiding Yu, Anima Anandkumar, Jose M Alvarez, and Ping Luo. Segformer: Simple and

efficient design for semantic segmentation with transformers. *Advances in neural information processing systems*, 34: 12077–12090, 2021. [2](#)

[53] Qi Xie, Qian Zhao, Zongben Xu, and Deyu Meng. Fourier series expansion based filter parametrization for equivariant convolutions. *IEEE Transactions on Pattern Analysis and Machine Intelligence*, 45(4):4537–4551, 2022. [1](#), [2](#)

[54] Qi Xie, Jiahong Fu, Zongben Xu, and Deyu Meng. Rotation equivariant arbitrary-scale image super-resolution. *IEEE Transactions on Pattern Analysis and Machine Intelligence*, 2025. [2](#)

[55] Renjun Xu, Kaifan Yang, Ke Liu, and Fengxiang He.  $e(2)$ -equivariant vision transformer. In *Uncertainty in Artificial Intelligence*, pages 2356–2366. PMLR, 2023. [1](#), [2](#)

[56] Roman Zeyde, Michael Elad, and Matan Protter. On single image scale-up using sparse-representations. In *International conference on curves and surfaces*, pages 711–730. Springer, 2010. [7](#)

[57] Jiale Zhang, Yulun Zhang, Jinjin Gu, Yongbing Zhang, Linghe Kong, and Xin Yuan. Accurate image restoration with attention retractable transformer. *arXiv preprint arXiv:2210.01427*, 2022. [7](#)

[58] Yulun Zhang, Kunpeng Li, Kai Li, Lichen Wang, Bineng Zhong, and Yun Fu. Image super-resolution using very deep residual channel attention networks. In *Proceedings of the European conference on computer vision (ECCV)*, pages 286–301, 2018. [8](#)

[59] Yulun Zhang, Yapeng Tian, Yu Kong, Bineng Zhong, and Yun Fu. Residual dense network for image super-resolution. In *Proceedings of the IEEE conference on computer vision and pattern recognition*, pages 2472–2481, 2018. [8](#)

[60] Bolei Zhou, Hang Zhao, Xavier Puig, Tete Xiao, Sanja Fidler, Adela Barriuso, and Antonio Torralba. Semantic understanding of scenes through the ade20k dataset. *International Journal of Computer Vision*, 127(3):302–321, 2019. [7](#)

[61] Shangchen Zhou, Jiawei Zhang, Wangmeng Zuo, and Chen Change Loy. Cross-scale internal graph neural network for image super-resolution. *Advances in neural information processing systems*, 33:3499–3509, 2020. [8](#)